Visualizing Molecular Wavefunctions Using Monte Carlo Methods

S. A. ALEXANDER,[1] R. L. COLDWELL[2]

[1]*Department of Physics, Southwestern University, Georgetown, TX 78626*

[2]*Department of Physics, University of Florida, Gainesville, FL 32611*

Received 4 January 2008; accepted 2 April 2008
Published online 2 September 2008 in Wiley InterScience (www.interscience.wiley.com).
DOI 10.1002/qua.21774

ABSTRACT: Using explicitly correlated wavefunctions and variational Monte Carlo we calculate the electron density, the electron density difference, the intracule density, the extracule density, two forms of the kinetic energy density, the Laplacian of the electron density, the Laplacian of the intracule density, and the Laplacian of the extracule density on a dense grid of points for the ground state of the hydrogen molecule at three internuclear distances (0.6, 1.4, 8.0). With these values we construct a contour plot of each function and describe how it can be used to visualize the distribution of electrons in this molecule. We also examine the influence of electron correlation on each expectation value by calculating each function with a Hartree–Fock wavefunction and then comparing these values with our explicitly correlated values.
 Int J Quantum Chem 109: 385–400, 2009

Key words: intracule density; extracule density; electron density; Laplacians

1. Introduction

Many concepts in chemistry are based on localized groups of electrons (e.g., atomic shells, binding and lone pairs, π and σ electrons). These concepts have been related to the results of quantum mechanical calculations through a wide variety of atomic and molecular functions [1–7]. The most widely used functions are the electron density

$$\rho(\mathbf{R}) = \sum_{i=1}^{N_{\text{elec}}} \int \Psi(\mathbf{r}_1 \ldots \mathbf{r}_{N_{\text{elec}}})^2 \delta(\mathbf{R} - \mathbf{r}_i) d\mathbf{r}_1 \ldots d\mathbf{r}_{N_{\text{elec}}} \quad (1)$$

the electron density difference

$$\Delta(\mathbf{R}) = \rho_{\text{molecular}}(\mathbf{R}) - \rho_{\text{atomic}}(\mathbf{R}) \quad (2)$$

the intracule (relative motion) density

$$\mathrm{I}(\mathbf{R}) = \sum_{i<j}^{N_{\text{elec}}} \int \Psi(\mathbf{r}_1 \ldots \mathbf{r}_{N_{\text{elec}}})^2 \delta(\mathbf{R} - \mathbf{r}_i + \mathbf{r}_j) d\mathbf{r}_1 \ldots d\mathbf{r}_{N_{\text{elec}}} \quad (3)$$

Correspondence to: S. A. Alexander; e-mail: alexands@southwestern.edu

the extracule (center of mass motion) density

$$E(\mathbf{R}) = \sum_{i<j}^{N_{elec}} \int \Psi(\mathbf{r}_1 \ldots \mathbf{r}_{N_{elec}})^2 \times \delta(\mathbf{R} - (\mathbf{r}_i + \mathbf{r}_j)/2) d\mathbf{r}_1 \ldots d\mathbf{r}_{N_{elec}} \quad (4)$$

and the two forms of the kinetic energy density

$$KE1(\mathbf{R}) = \sum_{i=1}^{N_{elec}} \int \sum_{j=1}^{N_{elec}} \nabla_j \Psi(\mathbf{r}_1 \ldots \mathbf{r}_{N_{elec}}) \bullet \nabla_j \Psi(\mathbf{r}_1 \ldots \mathbf{r}_{N_{elec}}) \times \delta(\mathbf{R} - \mathbf{r}_i) d\mathbf{r}_1 \ldots d\mathbf{r}_{N_{elec}} \quad (5)$$

$$KE2(\mathbf{R}) = -\sum_{i=1}^{N_{elec}} \int \sum_{j=1}^{N_{elec}} \Psi(\mathbf{r}_1 \ldots \mathbf{r}_{N_{elec}}) \nabla_j^2 \Psi(\mathbf{r}_1 \ldots \mathbf{r}_{N_{elec}}) \times \delta(\mathbf{R} - \mathbf{r}_i) d\mathbf{r}_1 \ldots d\mathbf{r}_{N_{elec}} \quad (6)$$

Previous studies (see for example Ref. [8]) suggest that those properties that include a two-electron delta function [e.g., Eqs. (3) and (4)] should be much more sensitive to the effects of electron correlation than those that include a one-electron delta function.

In this article we use variational Monte Carlo methods to visualize the distribution of electrons in the ground state of the hydrogen molecule at three internuclear distances (0.6, 1.4, 8.0). We describe how to calculate Eqs. (1)–(6) in Section 2. We then evaluate each expectation value on a dense grid of points, construct contour plots of these functions and interpret each plot. Because our wavefunctions are explicitly correlated, they capture a high percentage of the correlation energy and produce very accurate results. In Section 3, we investigate three additional functions that can provide some insight into the electronic structure of this molecule—the Laplacian of the electron density, the Laplacian of the intracule density, and the Laplacian of the extracule density. We begin by comparing two methods of computing these Laplacians. Using the most efficient method, we then create contour plots of each function. Next, we examine the effect of electron correlation on all of these expectation values by calculating each function with a Hartree–Fock wavefunction and then examining the differences between these values and our highly accurate values. This work is described in Section 4. Unless otherwise indicated, all values in this article are given in atomic units.

2. Calculating the Densities

Variational Monte Carlo is a method of computing the expectation value of an operator

$$< A > = \sum_i [\Psi(\mathbf{x}_i) A \Psi(\mathbf{x}_i)/w(\mathbf{x}_i)] / \sum_i [\Psi(\mathbf{x}_i)^2/w(\mathbf{x}_i)] \quad (7)$$

and its standard deviation (i.e., statistical error)

$$\sigma^2 = \sum_i [(A\Psi(\mathbf{x}_i) - < A > \Psi(\mathbf{x}_i))^2/w(\mathbf{x}_i)^2] / \{\sum_i [\Psi(\mathbf{x}_i)^2/w(\mathbf{x}_i)]\}^2 \quad (8)$$

using Monte Carlo integration. Here, $\Psi(\mathbf{x}_i)$ is the value of the trial wavefunction at the Monte Carlo integration point $\boldsymbol{x}_i$ and the weight function $w(\mathbf{x}_i)$ is the relative probability of choosing this point. In a variational Monte Carlo calculation the adjustable parameters in the trial wavefunction are often optimized with respect to a functional, usually some combination of the energy and its standard deviation [9, 10]. The Monte Carlo integration points used in these calculations are generated from a guiding function that can also be optimized with respect to the standard deviation of the local energy or any other property [11].

In Refs. [12] and [13] we showed that the trial wavefunction form

$$\Psi = (1 + P_{12})(1 + P_{AB}) \exp \times (\sum_{k=0} a_k q_{1A}^i q_{1B}^j q_{2A}^l q_{2B}^m q_{12}^n - \alpha \mathbf{r}_{1A} - \beta \mathbf{r}_{2B}) \quad (9)$$

produces rapidly convergent energies for the H_2 ground state. Here P_{12} is the operator which interchanges the two electrons, P_{AB} is the operator which interchanges the two nuclei and $q_x = r_x/(1 + cr_x)$ is a coordinate transformation which allows terms in the exponent to go smoothly to the separated atom limit. The exponents i, j, l, m, and n are integers (0, 1,. . .) which have been preselected for each value of k. In Ref. [12] we optimized a separate $N = i + j + l + m + n = 4$ wavefunction at 24 internuclear distances using variance minimization and 4,000 Monte Carlo integration points. With these wavefunctions we then computed the Born–Oppenheimer energy, the diagonal correction to the

TABLE I

A comparison of selected expectation values of H_2 ($X\ ^1\Sigma_g^+$) as a function of the size of the wavefunction, *N*.

N	$\rho(\mathbf{R})$ [Eq. (10)]	$\Delta(\mathbf{R})$ [Eq. (4)]	I(**R**) [Eq. (11)]	E(**R**) [Eq. (12)]	KE1(**R**) [Eq. (13)]	KE2(**R**) [Eq. (14)]
1	0.2636 (3)	0.1066 (3)	0.01631 (3)	0.4076 (6)	0.2774 (3)	0.971 (1)
2	0.2710 (3)	0.1140 (3)	0.01676 (3)	0.4110 (6)	0.2794 (3)	0.959 (1)
3	0.2725 (3)	0.1155 (3)	0.01681 (3)	0.4147 (6)	0.2822 (3)	0.971 (1)
4	0.2726 (3)	0.1156 (3)	0.01679 (3)	0.4148 (6)	0.2822 (3)	0.971 (1)
N	$\nabla^2\rho(\mathbf{R})$ [Eq. (18)]	$\nabla^2\rho(\mathbf{R})$ [Eq. (21)]	∇^2I(**R**) [Eq. (19)]	∇^2I(**R**) [Eq. (22)]	∇^2E(**R**) [Eq. (20)]	∇^2E(**R**) [Eq. (23)]
1	−1.388 (2)	−1.387 (2)	+9.13 (2)	−0.0657 (2)	−6.63 (1)	−6.64 (1)
2	−1.360 (1)	−1.359 (1)	+9.15 (1)	−0.0559 (1)	−6.75 (1)	−6.75 (1)
3	−1.379 (2)	−1.378 (2)	+9.76 (2)	−0.0554 (1)	−6.90 (1)	−6.91 (1)
4	−1.377 (2)	−1.376 (2)	+9.82 (2)	−0.0542 (1)	−6.91 (1)	−6.91 (1)

These properties are computed at the point **R** = (0, 0, 0) using 1,024,000 Monte Carlo integration points The value in the parenthesis is the statistical error. The atoms in this molecule are placed on the *x*-axis at $A_x = \pm 0.7$. All values are in a.u.

Born–Oppenheimer energy and the lowest-order relativistic energy [13]. All of these values were accurate to a microhartree or better. In a subsequent article, we used these same wavefunctions to calculate a wide variety of molecular properties [14].

In Ref. [15] we showed that one and two electron delta functions could be accurately and efficiently computed by fixing the position of one electron in the wavefunction and then integrating over the remaining electrons. Here, we use this same technique to transform Eqs. (1) and (3)–(6) into the following expressions

$$\rho(\mathbf{R}) = 2\int \Psi(\mathbf{r}_1 = \mathbf{R},\mathbf{r}_2)^2 d\mathbf{r}_2 \tag{10}$$

$$\mathrm{I}(\mathbf{R}) = \int \Psi(\mathbf{r}_1 = \mathbf{R} + \mathbf{r}_2,\mathbf{r}_2)^2 d\mathbf{r}_2 \tag{11}$$

$$\mathrm{E}(\mathbf{R}) = 8\int \Psi(\mathbf{r}_1 = 2\mathbf{R} - \mathbf{r}_2,\mathbf{r}_2)^2 d\mathbf{r}_2 \tag{12}$$

$$\mathrm{KE1}(\mathbf{R}) = 2\int [\nabla_1\Psi(\mathbf{r}_1 = \mathbf{R},\mathbf{r}_2)\bullet\nabla_1\Psi(\mathbf{r}_1 = \mathbf{R},\mathbf{r}_2) + \nabla_2\Psi(\mathbf{r}_1 = \mathbf{R},\mathbf{r}_2)\bullet\nabla_2\Psi(\mathbf{r}_1 = \mathbf{R},\mathbf{r}_2)]d\mathbf{r}_2 \tag{13}$$

$$\mathrm{KE2}(\mathbf{R}) = -2\int [\Psi(\mathbf{r}_1 = \mathbf{R},\mathbf{r}_2)\nabla_1^2\Psi(\mathbf{r}_1 = \mathbf{R},\mathbf{r}_2) + \Psi(\mathbf{r}_1 = \mathbf{R},\mathbf{r}_2)\nabla_2^2\Psi(\mathbf{r}_1 = \mathbf{R},\mathbf{r}_2)]d\mathbf{r}_2 \tag{14}$$

Equation (2) can be calculated from the difference between Eq. (10) and the analytic expression for the density of the hydrogen atom. As Table I shows, all of these expectation values converge quickly as a function of the size of the wavefunction, *N*. In Table II, we list the values of each expectation value at nine points in the plane of the molecule, i.e. **R** = (*x*, *y*, 0). These values were computed using our largest wavefunction at each internuclear distance and 1,024,000 Monte Carlo integration points. At A_x = 0.7 our values for the electron density and the electron density difference are in excellent agreement with the values given in Ref. [16]. For most of the other properties in Table II there are no published values with which we can compare. One exception is Ref. [17] which uses a CISD wavefunction to obtain I(0, 0, 0) = 0.0259 and E(0, 0, 0) = 0.367 at A_x = 0.7. Our results differ from theirs by 54% and 12%, respectively. Because the intracule density is the same as the two-electron delta function at the origin, i.e., $\langle \mathrm{I}(0,0,0)\rangle = \langle \delta(r_{12})\rangle$, we can also compare with two highly accurate values for this property [18, 19]. Our results are in excellent agreement with these calculations.

To visualize each three-dimensional expectation value, we first evaluated their values on an equally spaced 31 × 31 grid of points in the plane of the molecule, i.e. **R** = (*x*, *y*, 0). Only points in the first quadrant were considered and then the values at these points were reflected to the other quadrants to produce the final contour plots. All expectation values were computed using our largest wavefunction and 64,000 Monte Carlo integration points. We chose this relatively small number of integration

TABLE II

Selected expectation values of H_2 ($X\ ^1\Sigma_g^+$) computed at the point R = (*x*, *y*, 0).

x	*y*	ρ(**R**)	Δ(**R**)	I(**R**)	E(**R**)	KE1(**R**)	KE2(**R**)	$\nabla^2\rho$(**R**)	∇^2I(**R**)	∇^2E(**R**)
A_x = 0.3										
0.0	0.0	0.942(1)	0.592(1)	0.05079(8)	0.839(1)	1.443(2)	10.07(1)	−17.24(2)	−0.3331(8)	−22.09(4)
		0.93578	0.58640	0.10151	0.81209	1.74924	10.19516	−16.89183	−0.68444	−21.90216
				0.050837 [18]						
0.0	1.0	0.0974(1)	0.0185(1)	0.03618(8)	0.0522(2)	0.3787(4)	0.2467(4)	0.2645(3)	−0.062(1)	0.42(1)
		0.09792	0.01903	0.03973	0.05214	0.37311	0.24351	0.25920	−0.04683	0.37338
0.0	2.0	0.006334(7)	−0.004816(7)	0.00716(3)	0.000569(7)	0.02594(3)	0.01123(2)	0.02947(3)	0.0104(3)	0.0102(3)
		0.00635	−0.00480	0.00652	0.00074	0.02329	0.00844	0.02970	0.01167	0.01122
1.0	0.0	0.1238(1)	0.0217(1)	0.04318(8)	0.0607(2)	0.5066(6)	0.3787(5)	0.2565(3)	−0.136(1)	0.40(1)
		0.12383	0.02169	0.04581	0.06264	0.49953	0.37541	0.24824	−0.10925	0.36199
1.0	1.0	0.03398(4)	−0.00570(4)	0.02228(6)	0.00924(5)	0.1377(2)	0.0715(1)	0.1326(1)	−0.0136(8)	0.128(2)
		0.03404	−0.00564	0.02143	0.01040	0.12964	0.06308	0.13312	0.00209	0.11835
1.0	2.0	0.003478(4)	−0.003815(4)	0.00475(2)	0.000194(4)	0.01435(2)	0.00600(1)	0.01673(2)	0.0088(2)	0.0033(2)
		0.00347	−0.00382	0.00421	0.00027	0.01268	0.00426	0.01685	0.00900	0.00429
2.0	0.0	0.007419(8)	−0.006404(9)	0.00901(3)	0.000667(8)	0.03073(4)	0.01354(3)	0.03445(4)	0.0087(5)	0.0119(4)
		0.00738	−0.00644	0.00783	0.00089	0.02750	0.01024	0.03453	0.01131	0.01329
2.0	1.0	0.003804(4)	−0.004469(4)	0.00542(2)	0.000212(4)	0.01578(2)	0.00665(1)	0.01830(2)	0.0089(3)	0.0037(2)
		0.00378	−0.00449	0.00470	0.00030	0.01392	0.00473	0.01836	0.00930	0.00476
2.0	2.0	0.0007585(9)	−0.0016291(9)	0.001466(7)	0.0000115(5)	0.003164(4)	0.001240(3)	0.003854(4)	0.00442(8)	0.00024(1)
		0.00075	−0.00164	0.00130	0.00002	0.00271	0.00078	0.00385	0.00370	0.00034
A_x = 0.7										
0.0	0.0	0.2726(3)	0.1156(3)	0.01679(3)	0.4148(6)	0.2822(3)	0.971(1)	−1.376(2)	−0.0542(1)	−6.91(1)
		0.27295	0.11596	0.04322	0.34573	0.30736	1.00028	−1.38584	−0.16126	−5.16033
		0.27294 [16]	0.11557 [16]	0.0259 [17]	0.367 [17]				−0.0446 [17]	−5.940 [17]
				0.016774 [18]						
				0.0167434 [19]						
0.0	1.0	0.07332(8)	0.01790(8)	0.01787(4)	0.0557(1)	0.1598(2)	0.1275(2)	0.06490(9)	−0.0216(3)	0.175(5)
		0.07423	0.01881	0.02382	0.05212	0.15842	0.12925	0.05835	−0.02875	0.14181
		0.07341 [16]	0.01796 [16]							
0.0	2.0	0.00848(1)	−0.00071(1)	0.00642(2)	0.00147(1)	0.02166(2)	0.00901(2)	0.02534(3)	0.0020(1)	0.0169(3)
		0.00872	−0.00047	0.00652	0.00182	0.02038	0.07738	0.02529	0.00443	0.01716
		0.00848 [16]	−0.00072 [16]							
1.0	0.0	0.2106(2)	0.0253(2)	0.02671(5)	0.0872(2)	0.5811(6)	1.315(2)	−1.467(2)	−0.0798(5)	−0.187(5)
		0.20489	0.01957	0.03135	0.09882	0.57441	1.26624	−1.38365	−0.08748	−0.43712
		0.21087 [16]	0.02540 [16]							
1.0	1.0	0.04516(5)	−0.00045(5)	0.01687(4)	0.01733(6)	0.1148(1)	0.0772(1)	0.07542(8)	−0.0225(3)	0.112(2)
		0.04484	−0.00077	0.01786	0.01951	0.10900	0.07197	0.07405	−0.01580169	0.10021
		0.04523 [16]	−0.00033 [16]							

TABLE II
(Continued)

x	y	$\rho(\mathbf{R})$	$\Delta(\mathbf{R})$	I($\mathbf{R}$)	E($\mathbf{R}$)	KE1($\mathbf{R}$)	KE2($\mathbf{R}$)	$\nabla^2\rho(\mathbf{R})$	∇^2I($\mathbf{R}$)	∇^2E($\mathbf{R}$)
1.0	2.0	0.005720(7)	−0.001526(7)	0.00541(2)	0.000650(7)	0.01502(2)	0.00594(1)	0.01821(2)	0.0027(1)	0.0077(2)
		0.00583	−0.00141	0.00508	0.00089	0.01387	0.00477	0.01819	0.00425589	0.00898
		0.00573 [16]	−0.00152 [16]							
2.0	0.0	0.01768(2)	−0.00740(2)	0.01526(3)	0.00271(1)	0.04864(5)	0.02514(4)	0.04709(5)	−0.0289(3)	0.0271(4)
		0.01717	−0.00791	0.01235	0.00392	0.04381	0.02085	0.04592	−0.01366001	0.03151
		0.01770 [16]	−0.00745 [16]							
2.0	1.0	0.00867(1)	−0.00431(1)	0.00926(2)	0.000933(7)	0.02360(3)	0.01027(2)	0.02673(3)	−0.0044(2)	0.0106(4)
		0.00854	−0.00444	0.00757	0.00141	0.02121	0.00814	0.02615	0.00058485	0.01338
		0.00868 [16]	−0.00431 [16]							
2.0	2.0	0.001817(2)	−0.001264(2)	0.00292(1)	0.000071(1)	0.004936(6)	0.001710(4)	0.006464(7)	0.00307(7)	0.00100(4)
		0.00184	−0.00124	0.00244	0.00012	0.00443	0.00123	0.00640	0.00313162	0.00141
		0.00182 [16]	−0.00126 [16]							
$A_x = 4.0$										
0.0	0.0	0.0002185(3)	0.0000050(3)	0.000000329(2)	0.3178(4)	0.0004253(6)	0.0001075(3)	0.0006359(8)	0.000000355(2)	−5.096(9)
		0.00136	0.00115	0.01130	0.09040	0.00093	0.00075	0.00036	−0.03738	−1.19607
				0.0000003 [18]						
0.0	2.0	0.0000850(1)	0.0000020(1)	0.000000449(2)	0.00318(2)	0.0001660(2)	0.0000372(1)	0.0002578(3)	0.000000556(3)	0.0205(9)
		0.00067	0.00059	0.00299	0.00264	0.00054	0.00035	0.00038	−0.00039	0.00815
0.0	4.0	0.00000795(1)	0.00000019(1)	0.000000171(1)	0.0000035(1)	0.00001561(2)	0.000002704(9)	0.00002583(3)	0.000000238(2)	0.0000388(7)
		0.00011	0.00011	0.00033	0.00002	0.00011	0.00005	0.00012	0.00025	0.00011
2.0	0.0	0.00583(1)	−0.00001(1)	0.00000627(4)	0.00336(2)	0.01163(2)	0.00583(1)	0.01162(2)	0.0000174(1)	0.0204(5)
		0.00715	0.00132	0.00314	0.00590	0.00844	0.00565	0.00558	−0.00058	0.00702
2.0	2.0	0.001113(2)	−0.000002(2)	0.00000403(3)	0.000220(2)	0.002221(4)	0.000787(2)	0.002872(5)	0.00000968(8)	0.00187(6)
		0.00202	0.00091	0.00133	0.00083	0.00231	0.00122	0.00218	0.00041	0.00248
2.0	4.0	0.00004179(8)	0.00000008(8)	0.00000103(1)	0.00000064(2)	0.0000832(2)	0.00001862(7)	0.0001296(2)	0.00000232(3)	0.0000077(2)
		0.00018	0.00014	0.00021	0.00001	0.00021	0.00008	0.00025	0.00017	0.00006
4.0	0.0	0.3175(6)	−0.0008(6)	0.000194(1)	0.00000503(7)	0.635(1)	500.0	−500.0	0.00032(1)	0.0000428(5)
		0.21546	−0.10285	0.00074	0.04511	0.14756	54.80313	−109.31114	0.00022	−0.59756
4.0	2.0	0.00582(1)	−0.00001(1)	0.0000939(8)	0.00000081(2)	0.01163(2)	0.00582(1)	0.01163(2)	0.000175(2)	0.0000085(2)
		0.00599	0.00016	0.00043	0.00130	0.00812	0.00462	0.00701	0.00019	0.00409
4.0	4.0	0.0001066(2)	−0.0000002(2)	0.0000140(2)	0.0000000102(7)	0.0002131(4)	0.0000534(2)	0.0003197(6)	0.0000296(7)	0.000000125(6)
		0.00026	0.00015	0.00010	0.00001	0.00033	0.00012	0.00043	0.00008	0.00005

The top value is from our Monte Carlo calculation using our largest wavefunction and 1,024,000 Monte Carlo integration points. The value in the parenthesis is the statistical error. The second number is from our Hartree–Fock calculation. The atoms in this molecule are placed on the x-axis at $\pm A_x$. All values are in a.u.

TABLE III

Extrema found along the internuclear axis of the H_2 ground state from $x = [0,\infty]$.

	$A_x = 0.3$	$A_x = 0.7$	$A_x = 4.0$
$\rho(\mathbf{R})$	Min $x = 0.0$: 0.943(4)	Min $x = 0.0$: 0.273(1)	Min $x = 0.0$: 0.000221(1)
	Max $x = 0.3$: 1.068(5)	Max $x = 0.7$: 0.459(2)	Max $x = 4.0$: 0.320(2)
$\Delta(\mathbf{R})$	Min $x = 0.0$: 0.593(4)	Min $x = 0.0$: 0.116(1)	Min $x = 0.0$: 0.000001(1)
	Max $x = 0.3$: 0.654(5)	Max $x = 0.7$: 0.122(2)	Max $x = 4.0$: 0.002(2)
	Min $x = 1.6$: $-0.0085(1)$	Min $x = 1.7$: $-0.0091(2)$	
$I(\mathbf{R})$	Min $x = 0.0$: 0.0509(3)	Min $x = 0.0$: 0.0168(1)	Min $x = 0.0$: $3.33(7) \times 10^{-7}$
	Max $x = 0.4$: 0.0619(4)	Max $x = 1.0$: 0.0269(2)	Max $x = 8.0$: 0.0203(1)
$E(\mathbf{R})$	Max $x = 0.0$: 0.841(5)	Max $x = 0.0$: 0.416(2)	Max $x = 0.0$: 0.322(2)
$KE1(\mathbf{R})$	Min $x = 0.0$: 1.445(7)	Min $x = 0.0$: 0.283(1)	Min $x = 0.0$: 0.000430(2)
	Max $x = 0.3$: 4.39(2)	Max $x = 0.7$: 1.275(6)	Max $x = 4.0$: 0.641(5)
$KE2(\mathbf{R})$	Min $x = 0.0$: 10.08(4)	Min $x = 0.0$: 0.973(4)	Min $x = 0.0$: 0.000109(1)
	Max $x = 0.3$: 500.0	Max $x = 0.7$: 500.0	Max $x = 4.0$: 500.0
$\nabla^2\rho(\mathbf{R})$	Max $x = 0.0$: $-17.26(8)$	Max $x = 0.0$: $-1.378(6)$	Min $x = 0.0$: 0.000643(3)
	Min $x = 0.3$: -500.0	Min $x = 0.7$: -500.0	Max $x = 2.6$: 0.0222(2)
	Max $x = 1.0$: 0.257(1)	Max $x = 1.6$: 0.0718(3)	Min $x = 4.0$: -500.0
			Max $x = 5.4$: 0.0223(2)
$\nabla^2 I(\mathbf{R})$	Min $x = 0.0$: $-0.331(3)$	Min $x = 0.0$: $-0.0539(6)$	Min $x = 0.0$: $3.57(9) \times 10^{-7}$
	Max $x = 0.1$: 0.594(4)	Max $x = 0.1$: 0.270(2)	Max $x = 5.6$: 0.0015(2)
	Min $x = 0.6$: $-0.282(4)$	Min $x = 1.3$: $-0.093(1)$	Min $x = 8.0$: $-0.0809(8)$
	Max $x = 2.3$: 0.0100(6)	Max $x = 3.4$: 0.0031(1)	Max $x = 10.4$: 0.0016(2)
$\nabla^2 E(\mathbf{R})$	Min $x = 0.0$: $-22.1(2)$	Min $x = 0.0$: $-6.91(5)$	Min $x = 0.0$: $-5.14(3)$
	Max $x = 1.0$: 0.41(4)	Max $x = 1.4$: 0.110(7)	Max $x = 1.2$: 0.09(1)

All values have been calculated using our largest wavefunction and 64,000 Monte Carlo integrations points. The atoms in this molecule are placed at $\pm A_x$. All values are in a.u.

points in order to keep our computational costs low and because it determines most expectation values to about three significant digits—an accuracy that seems to produce decent plots. For each of our functions we list the extrema found along the internuclear axis in Table III.

As expected, our electron density plots in Figure 1 are very similar to those produced by other methods [3, 16, 20, 21]. At small internuclear distances most of the electron density in this molecule is concentrated around each atom (the maximum value is located on the nucleus) but there is also a substantial amount between the nuclei. It is this accumulation of negative charge that is responsible for the formation of the chemical bond. When the internuclear distance is large, however, almost all of the electron density is centered on the atoms and only a negligible amount of accumulation is left between the nuclei.

In an electron density difference plot, positive regions represent a movement of electron density away from the atoms and into areas that enable the molecule to exist in a state of electrostatic equilibrium. Such areas are often associated with chemical bonds (see for example Ref. [2]). Figure 2 shows that at small internuclear distances we get a large positive electron density difference between the nuclei and a smaller negative electron density difference behind each atom. This plot is very similar to those found in Refs. [3] and [16]. When the internuclear distance is large, we find a very small, positive electron density difference between the nuclei. This picture is significantly different than the one displayed in Ref. [2] where a small positive density difference (whose maximum value is $\sim$0.0002) is located between the nuclei and a small negative density difference is located behind each atom. The reason for this disagreement is likely due to the simple two-configuration wavefunction from Ref. [22] that was used to calculate the electron density.

For $A_x = 0.3$ and 0.7 our intracule density has a local minimum at the origin, it then increases along the internuclear axis until it reaches a maximum at almost exactly midway between A_x and $2A_x$ and then drops quickly to 0 for large values of x. Be-

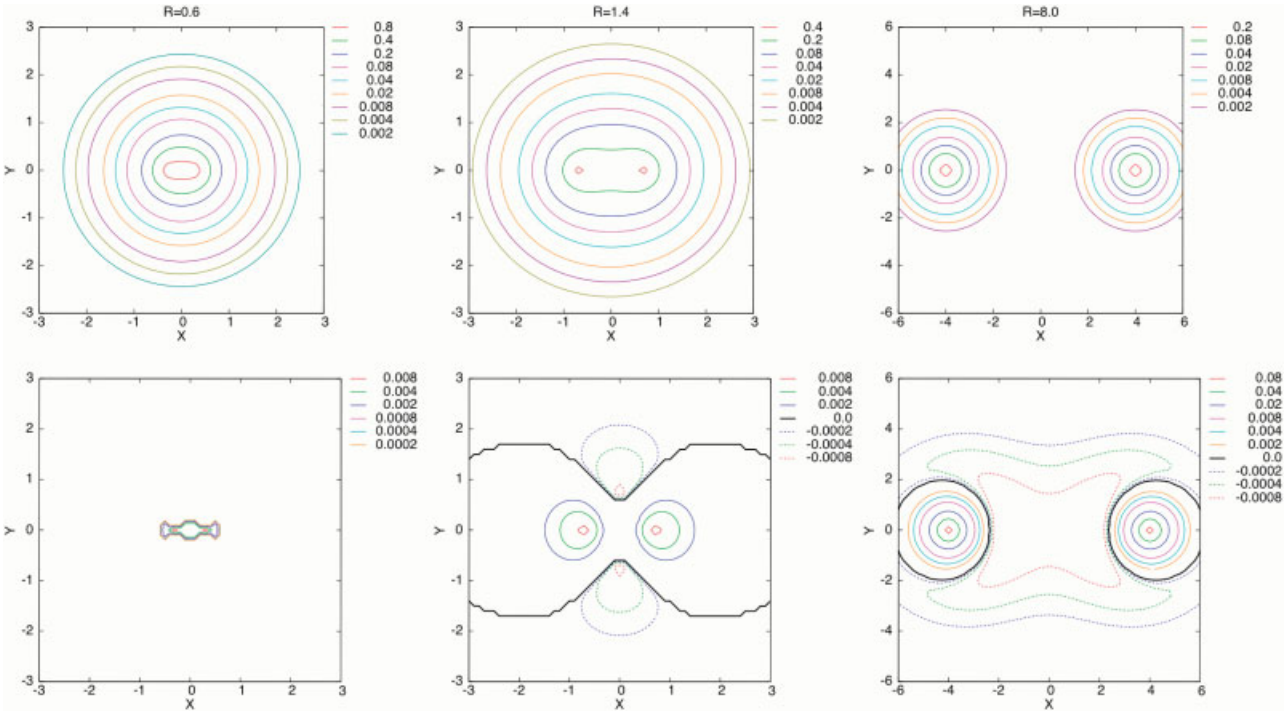

FIGURE 1. Plots of the H_2 ($X\ ^1\Sigma_g^+$) electron density $\rho(x, y, 0)$. The values in the top row are computed using Eq. (10), our largest Monte Carlo wavefunction and 64,000 Monte Carlo integration points. The values in the bottom row are the difference between our Monte Carlo results and the electron density computed using a Hartree–Fock wavefunction. The atoms in this molecule are placed on the x-axis at $\pm R/2$. All values are in a.u. [Color figure can be viewed in the online issue, which is available at www.interscience.wiley.com.]

cause the intracule measures the relative motion of an electron pair, placing two electrons on the same atom leads to a maximum at the origin ($A_x - A_x = 0$); placing one electron on each atom produces a maximum at twice the internuclear distance ($A_x - (-A_x) = 2A_x$). The locations of these maxima suggest that the electrons are grouped between the atoms—a traditional covalent structure. For $A_x = 4.0$ our intracule density has a small local minimum at the origin, it then increases along the internuclear axis until it reaches a maximum value at twice the nuclear position ($2A_x$) and then drops quickly to zero. The location of this maximum clearly suggests a pure ionic structure.

There are only two plots of the intracule in the literature (both at $A_x = 0.7$) with which we can compare with Figure 3. The one in Ref. [17] has maxima at ± 0.92 (which is close to our value of ± 1.0) but a very different shape around the origin. Since we use the same contour intervals as Ref. [17], this disagreement is likely due to the substantial difference in our values for I(0, 0, 0). In contrast, our plot is in good agreement with the one in Ref. [23] except for small differences around the origin.

At all three internuclear distances our extracule plots, Figure 4, have a single maximum at the origin and are slightly broader along the internuclear axis, x, than in y. This deviation from a circular distribution is due to polarization of the atoms. The plot at $A_x = 0.7$ is very similar in appearance to the one in Ref. [17]. With the extracule alone, we cannot extract much insight about this molecule because two electrons on opposite sides of the origin will always produce a maximum at the origin ($(x+(-x))/2 = 0$). It is only by combining our extracule results and intracule results that we can produce a clear picture of where the electrons are: at $A_x = 0.3$ the most probable location is at ± 0.2, at $A_x = 0.7$ the most probable location is at ± 0.5 and at $A_x = 4.0$ the most probable location is at ± 4.0. This is in complete agreement with the traditional chemical picture of this molecule; a covalent structure at small internuclear distances and an ionic structure at large internuclear distances.

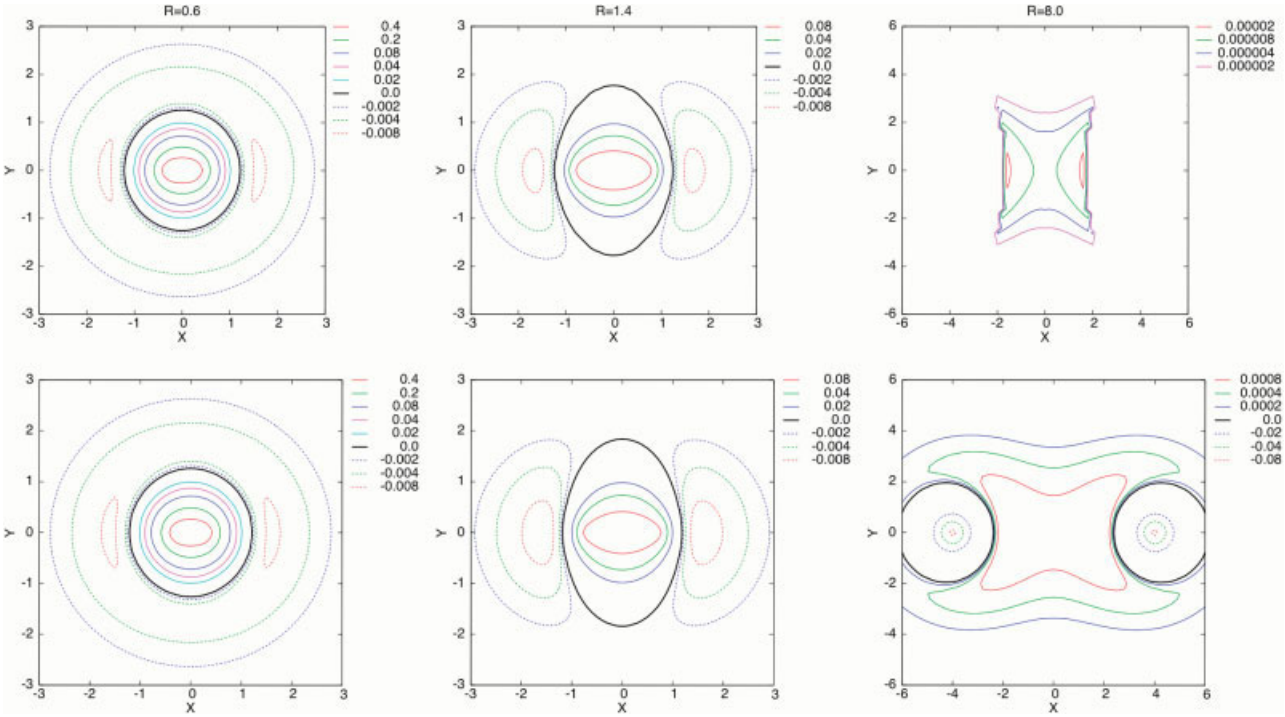

FIGURE 2. Plots of the H_2 ($X\ ^1\Sigma_g^+$) electron density difference $\Delta(x, y, 0)$. The values in the top row are computed using Eq. (2), our largest Monte Carlo wavefunction and 64,000 Monte Carlo integration points. The electron density differences in the bottom row are computed using a Hartree–Fock wavefunction. The atoms in this molecule are placed on the x-axis at $\pm R/2$. All values are in a.u. [Color figure can be viewed in the online issue, which is available at www.interscience.wiley.com.]

The two forms of the kinetic energy density correspond to the two mathematically equivalent ways of calculating the kinetic energy. KE1(**R**) should be large in those regions of space where the electron density is large. Figure 5 shows that this function is very similar in appearance to Figure 1 and has a moderate maximum at the two atomic positions. In contrast, KE2(**R**) corresponds to the average response of the wavefunction to the potential. Figure 6 shows that this function has a large maximum at the two atomic positions (whose values we capped at +500 for the purposes of plotting). When these two forms are integrated over all space, their values should be identical. Any statistically significant differences are a clear indication of integration problems.

3. Calculating the Derivatives of the Densities

Each of the densities in the previous section provides some insight into the electronic structure of the H_2 ground state. In larger systems, however, the results of these functions are often difficult to interpret since different electron–electron interactions can contribute to the same point in space. In such situations the Laplacian of these densities has proven to be an effective method of extracting insight

$$\nabla^2_{\mathbf{R}}\rho(\mathbf{R}) = \nabla^2_{\mathbf{R}}\Big[\sum_{i=1}^{N_{\text{elec}}}\int \Psi(\mathbf{r}_1\ldots\mathbf{r}_N)^2\delta(\mathbf{R}-\mathbf{r}_i)\mathrm{d}\mathbf{r}_1\ldots\mathrm{d}\mathbf{r}_{N_{\text{elec}}}\Big] \tag{15}$$

$$\nabla^2_{\mathbf{R}}\mathrm{I}(\mathbf{R}) = \nabla^2_{\mathbf{R}}\Big[\sum_{i<j} N_{\text{elec}}\int \Psi(\mathbf{r}_1\ldots\mathbf{r}_N)^2 \times \delta(\mathbf{R}-\mathbf{r}_i+\mathbf{r}_j)\mathrm{d}\mathbf{r}_1\ldots\mathrm{d}\mathbf{r}_{N_{\text{elec}}}\Big] \tag{16}$$

$$\nabla^2_{\mathbf{R}}\mathrm{E}(\mathbf{R}) = \nabla^2_{\mathbf{R}}\Big[\sum_{i<j}^{N_{\text{elec}}}\int \Psi(\mathbf{r}_1\ldots\mathbf{r}_N)^2 \times \delta(\mathbf{R}-(\mathbf{r}_i+\mathbf{r}_j)/2)\mathrm{d}\mathbf{r}_1\ldots\mathrm{d}\mathbf{r}_{N_{\text{elec}}}\Big] \tag{17}$$

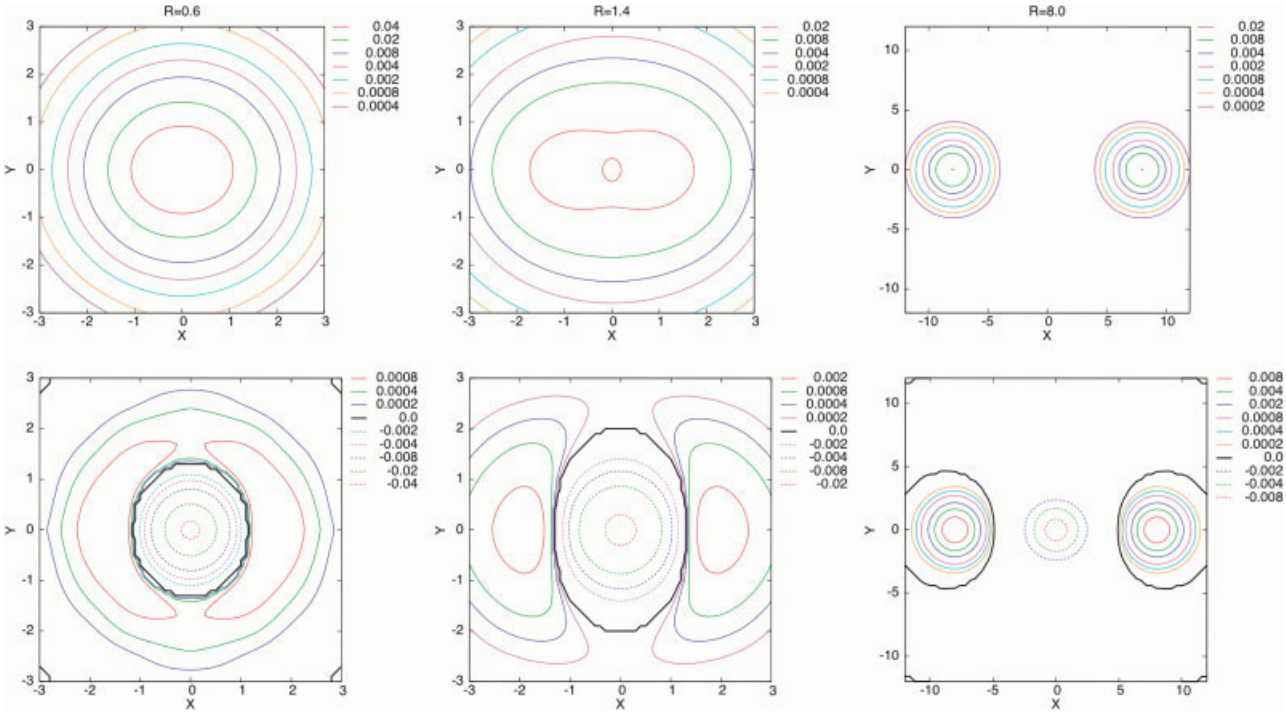

FIGURE 3. Plots of the H_2 ($X\ ^1\Sigma_g^+$) intracule density I(x, y, 0). The values in the top row are computed using Eq. (11), our largest Monte Carlo wavefunction and 64,000 Monte Carlo integration points. The values in the bottom row are the difference between our Monte Carlo results and the intracule density computed using a Hartree–Fock wavefunction. The atoms in this molecule are placed on the x-axis at $\pm R/2$. All values are in a.u. [Color figure can be viewed in the online issue, which is available at www.interscience.wiley.com.]

Because each of our densities is positive definite, a positive Laplacian denotes a region where the density is depleted and a negative Laplacian denotes a region where the density is concentrated.

In several recent studies, we have used standard numerical difference formulas to evaluate the derivatives of the energy and the wavefunction [12, 13, 24]. For H_2 this approach produces the following expressions for the Laplacians of the electron, intracule and extracule densities:

$$\nabla^2_{\mathbf{R}}\rho(R_x,R_y,R_z) = 2\int[\Psi(R_x+\Delta,R_y,R_z,\mathbf{r}_2)^2 + \Psi(R_x-\Delta,R_y,R_z,\mathbf{r}_2)^2 + \Psi(R_x,R_y+\Delta,R_z,\mathbf{r}_2)^2 + \Psi(R_x,R_y-\Delta,R_z,\mathbf{r}_2)^2 + \Psi(R_x,R_y,R_z+\Delta,\mathbf{r}_2)^2 + \Psi(R_x,R_y,R_z-\Delta,\mathbf{r}_2)^2 - 6\Psi(R_x,R_y,R_z,\mathbf{r}_2)^2]/\Delta^2 d\mathbf{r}_2 \quad (18)$$

$$\nabla^2_{\mathbf{R}}\mathrm{I}(R_x,R_y,R_z) = \int[\Psi((R_x+\Delta)+x_2,R_y+y_2,R_z+z_2,\mathbf{r}_2)^2 + \Psi((R_x-\Delta)+x_2,R_y+y_2,R_z+z_2,\mathbf{r}_2)^2 + \Psi(R_x+x_2,(R_y+\Delta)+y_2,R_z+z_2,\mathbf{r}_2)^2 + \Psi(R_x+x_2,(R_y-\Delta)+y_2,(R_z+z_2,\mathbf{r}_2)^2 + \Psi(R_x+x_2,R_y+y_2,(R_z+\Delta)+z_2,\mathbf{r}_2)^2 + \Psi(R_x+x_2,R_y+y_2,(R_z-\Delta)+z_2,\mathbf{r}_2)^2 - 6\Psi(R_x+x_2,R_y+y_2,R_z+z_2,\mathbf{r}_2)^2]/\Delta^2 d\mathbf{r}_2 \quad (19)$$

$$\nabla^2_{\mathbf{R}}\mathrm{E}(R_x,R_y,R_z) = 8\int[\Psi(2(R_x+\Delta)-x_2,2R_y-y_2,2R_z-z_2,\mathbf{r}_2)^2 + \Psi(2(R_x-\Delta)-x_2,2R_y-y_2,2R_z-z_2,\mathbf{r}_2)^2 + \Psi(2R_x-x_2,2(R_y+\Delta)-y_2,2R_z-z_2,\mathbf{r}_2)^2 + \Psi(2R_x-x_2,2(R_y-\Delta)-y_2,2R_z-z_2,\mathbf{r}_2)^2 + \Psi(2R_x-x_2,2R_y-y_2,2(R_z+\Delta)-z_2,\mathbf{r}_2)^2 + \Psi(2R_x-x_2,2R_y-y_2,2(R_z-\Delta)-z_2,\mathbf{r}_2)^2 - 6\Psi(2R_x-x_2,2R_y-y_2,2R_z-z_2,\mathbf{r}_2)^2]/\Delta^2 d\mathbf{r}_2 \quad (20)$$

Since a numerical Laplacian requires seven evaluations of the wavefunction, computing Eqs. (18)–

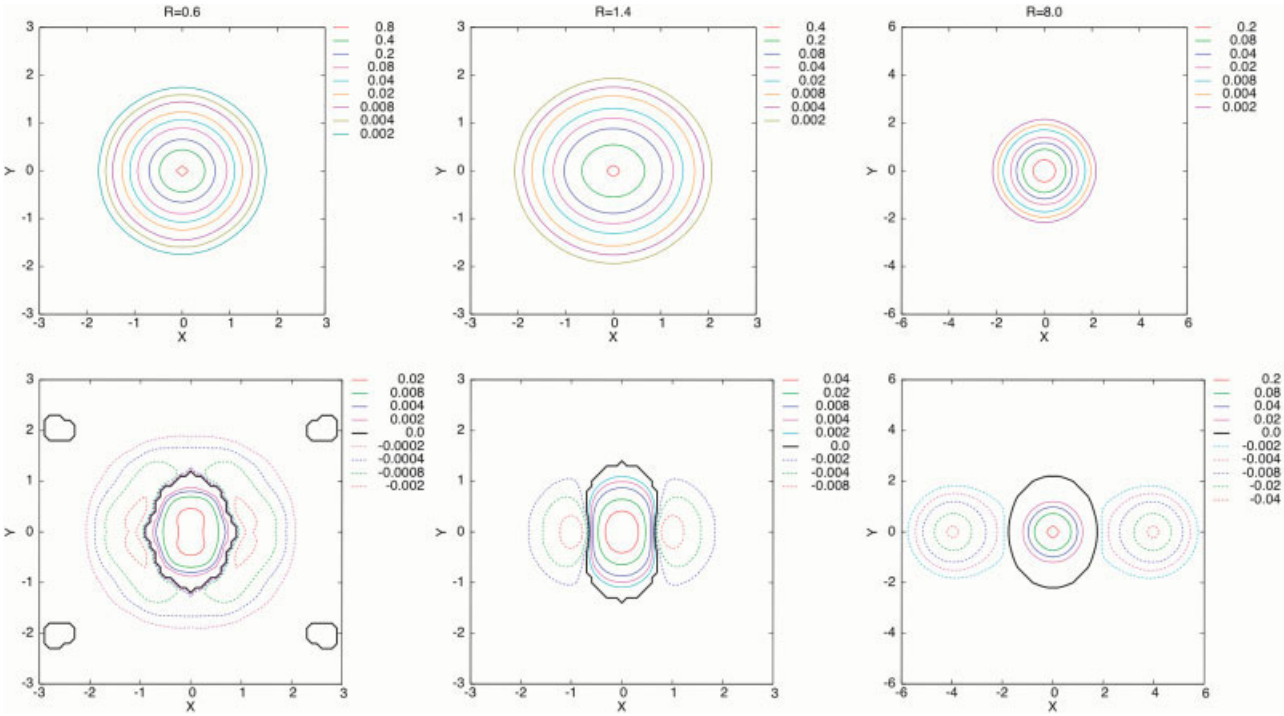

FIGURE 4. Plots of the H_2 ($X\ ^1\Sigma_g^+$) extracule density E(x, y, 0). The values in the top row are computed using Eq. (12), our largest Monte Carlo wavefunction and 64,000 Monte Carlo integration points. The values in the bottom row are the difference between our Monte Carlo results and the extracule density computed using a Hartree–Fock wavefunction. The atoms in this molecule are placed on the x-axis at $\pm R/2$. All values are in a.u. [Color figure can be viewed in the online issue, which is available at www.interscience.wiley.com.]

(20) on a dense grid of points will only be practical for small systems. One alternative is to rewrite the Laplacian of these densities as the Laplacian of the wavefunction

$$\nabla^2_{\mathbf{R}}\rho(\mathbf{R}) = 2\int \nabla^2_{\mathbf{R}}\Psi(\mathbf{r}_1 = \mathbf{R},\mathbf{r}_2)^2 d\mathbf{r}_2 = 2\int \nabla^2_1\Psi(\mathbf{r}_1 = \mathbf{R},\mathbf{r}_2)^2 d\mathbf{r}_2 = 4\int [\Psi(\mathbf{r}_1 = \mathbf{R},\mathbf{r}_2)\nabla^2_1\Psi(\mathbf{r}_1 = \mathbf{R},\mathbf{r}_2) + \nabla_1\Psi(\mathbf{r}_1 = \mathbf{R},\mathbf{r}_2)\bullet\nabla_1\Psi(\mathbf{r}_1 = \mathbf{R},\mathbf{r}_2)]d\mathbf{r}_2 \quad (21)$$

$$\nabla^2_{\mathbf{R}}I(\mathbf{R}) = \int \nabla^2_{\mathbf{R}}\Psi(\mathbf{r}_1 = \mathbf{R} + \mathbf{r}_2,\mathbf{r}_2)^2 d\mathbf{r}_2 = \int \nabla^2_1\Psi \times (\mathbf{r}_1 = \mathbf{R} + \mathbf{r}_2,\mathbf{r}_2)^2 d\mathbf{r}_2 = 2\int [\Psi(\mathbf{r}_1 = \mathbf{R} + \mathbf{r}_2,\mathbf{r}_2)\nabla^2_1\Psi \times (\mathbf{r}_1 = \mathbf{R} + \mathbf{r}_2,\mathbf{r}_2) + \nabla_1\Psi(\mathbf{r}_1 = \mathbf{R} + \mathbf{r}_2,\mathbf{r}_2)\bullet\nabla_1\Psi \times (\mathbf{r}_1 = \mathbf{R} + \mathbf{r}_2,\mathbf{r}_2)]d\mathbf{r}_2 \quad (22)$$

$$\nabla^2_{\mathbf{R}}E(\mathbf{R}) = 8\int \nabla^2_{\mathbf{R}}\Psi(\mathbf{r}_1 = 2\mathbf{R} - \mathbf{r}_2,\mathbf{r}_2)^2 d\mathbf{r}_2 = 32\int \nabla^2_1\Psi \times (\mathbf{r}_1 = 2\mathbf{R} - \mathbf{r}_2,\mathbf{r}_2)^2 d\mathbf{r}_2 = 64\int [\Psi(\mathbf{r}_1 = 2\mathbf{R} - \mathbf{r}_2,\mathbf{r}_2) \times \nabla^2_1\Psi(\mathbf{r}_1 = 2\mathbf{R} - \mathbf{r}_2,\mathbf{r}_2) + \nabla_1\Psi(\mathbf{r}_1 = 2\mathbf{R} - \mathbf{r}_2,\mathbf{r}_2) \bullet \nabla_1\Psi(\mathbf{r}_1 = 2\mathbf{R} - \mathbf{r}_2,\mathbf{r}_2)]d\mathbf{r}_2 \quad (23)$$

The main advantage of this approach is that only one evaluation of the wavefunction is needed at each grid point for each function. The additional increase in the overall computational cost due to the calculation of the derivatives of the wavefunction is small compared with the cost of just the wavefunction. In Table I we compare both methods of calculating the Lapacians. With one exception, these two approaches converge quickly and are in excellent agreement with one another. The reason that we get two different values for the Laplacian of the intracule is because the intracule at the origin is

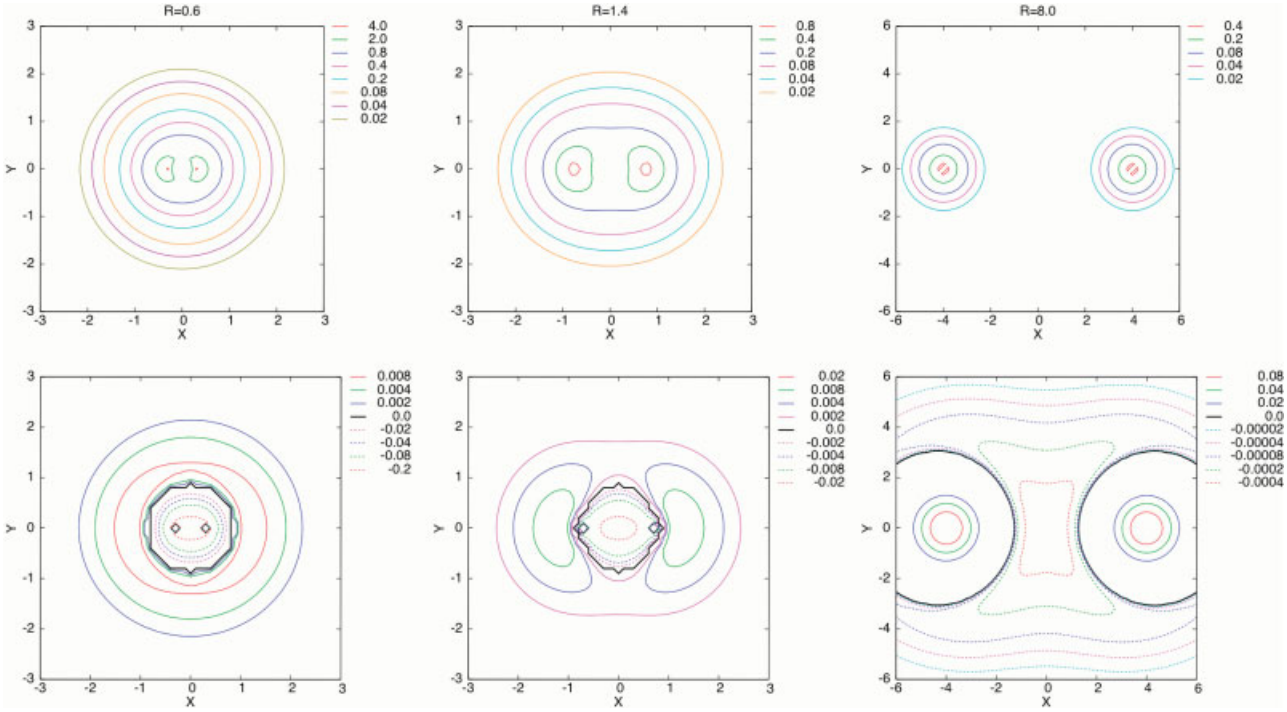

FIGURE 5. Plots of the H_2 ($X\ ^1\Sigma_g^+$) first kinetic energy density KE1(x, y, 0). The values in the top row are computed using Eq. (13), our largest Monte Carlo wavefunction and 64,000 Monte Carlo integration points. The values in the bottom row are the difference between our Monte Carlo results and the kinetic energy density computed using a Hartree–Fock wavefunction. The atoms in this molecule are placed on the x-axis at $\pm R/2$. All values are in a.u. [Color figure can be viewed in the online issue, which is available at www.interscience.wiley.com.]

the same as the two-electron delta function. For a wavefunction that exactly satisfies the electron–electron coalescence cusp this Laplacian is undefined. As our wavefunctions are highly accurate, our numerical difference formula is unable to compute an accurate value for this function with a moderate step size ($\Delta = 0.01$). At all other values of R we get superb agreement between these two methods. In Table II we list the results of Eqs. (21)–(23) at nine points in the plane of the molecule, i.e. $\mathbf{R} = (x, y, 0)$. These values were computed using our largest wavefunction at each internuclear distance and 1,024,000 Monte Carlo integration points.

We constructed contour plots of Eqs. (21)–(23) from the values of each function at the same 961 points as before, our largest wavefunctions and 64,000 Monte Carlo integration points. For each of these functions we list the extrema found along the internuclear axis in Table III. Figure 7 shows our plot of the Laplacian of the electron density. Along the internuclear axis two slightly different forms describe the behavior of this function. At $A_x = 0.3$ and 0.7 it has a small negative value at the origin, drops to a large negative value (which we capped at -500 for the purposes of plotting) at the atomic position, increases until it reaches a positive maximum and then drops to zero at large x. At $A_x = 4.0$ this function has a small positive local minimum at the origin, quickly increases to some maximum value, drops to a large negative value (which we capped at -500 for the purposes of plotting) at the atomic position, increases until it reaches a positive maximum and then drops to zero at large x.

In numerous papers Bader, Gillespie, and Popelier have shown that the Laplacian of the electron density duplicates the number and location of spatially localized electron pairs (see for example Refs. 2 and 3). Within each region where this Laplacian is negative an ionic bond will have no maxima and a covalent bond will have one or more maxima (the point at which there is a maximum probability of finding a pair of opposite spin electrons). This is precisely what we see in Figure 7. At small internuclear distances, the negative region between the atoms has a single maximum at the origin. At large

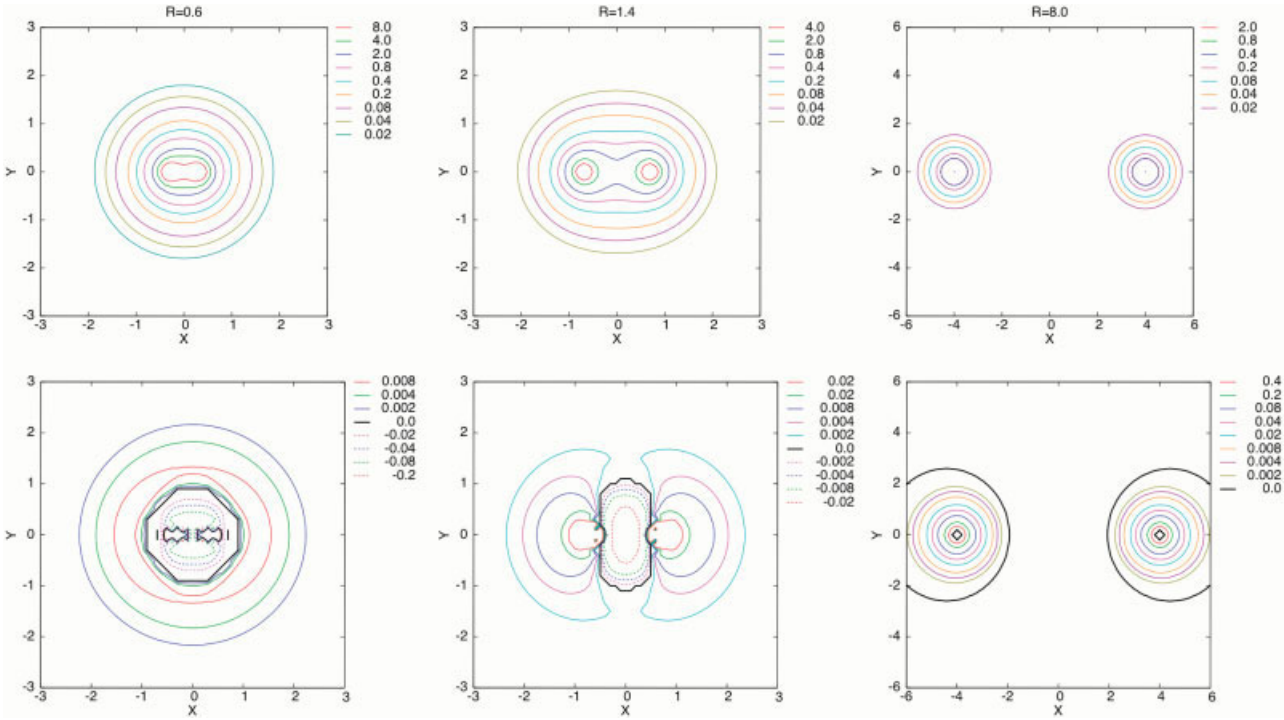

FIGURE 6. Plots of the H_2 ($X\ ^1\Sigma_g^+$) second kinetic energy density KE2(x, y, 0). The values in the top row are computed using Eq. (14), our largest Monte Carlo wavefunction and 64,000 Monte Carlo integration points. The values in the bottom row are the difference between our Monte Carlo results and the kinetic energy density computed using a Hartree–Fock wavefunction. The atoms in this molecule are placed on the x-axis at $\pm R/2$. All values are in a.u. [Color figure can be viewed in the online issue, which is available at www.interscience.wiley.com.]

internuclear distances, a negative region surrounds each atom but they are not connected and they contain no maxima.

Figure 8 shows our plot of the Laplacian of the intracule density. Unlike the Laplacian of the electron density, the behavior of this function along the internuclear axis has the same basic form at each of the internuclear distances we investigated. It has a local minimum at the origin, immediately increases to a positive maximum, drops to a negative minimum around $2A_x$, increases to a second positive maximum and then decreases to zero at large x. Our plot of the Laplacian of the intracule density has a noticeably different shape around the origin than the one in Ref. [17]. Where we get a region containing both positive and negative values they get a region with only negative values. This difference is obviously related to the accuracy with which our respective wavefunctions reproduce the correct electron–electron cusp coalescence.

In contrast, to the large number of papers that have discussed the merits of the Laplacian of the electron density, only a small number of studies have examined the Laplacians of the intracule or the extracule. In Ref. [25] Sarasola et al. showed that atomic shell structure was reproduced by the odd numbered zeros of the Laplacian of the extracule or by the radii corresponding to the mimima in the Laplacian of the intracule. Recently, Fradera et al. showed that the minima of these operators could be used to characterize the electron–electron interactions in molecules by identifying them with specific valence bond structures [17, 26]. If we use Fradera's results to help interpret Figure 8 then at small internuclear distances the tiny minimum around the origin represents a structure with two electrons on the same atom and the minimum at $\sim 2A_x$ describes a structure with a single electron on each atom. At large internuclear distances, there are two unconnected negative regions. The only minima are those at $2A_x$ and these clearly represent an ionic structure. When we compare the ambiguous information that we obtained about this molecule from the intracule with the more detailed information that we get from the Laplacian of the intracule, we can see the obvious advantages of the latter.

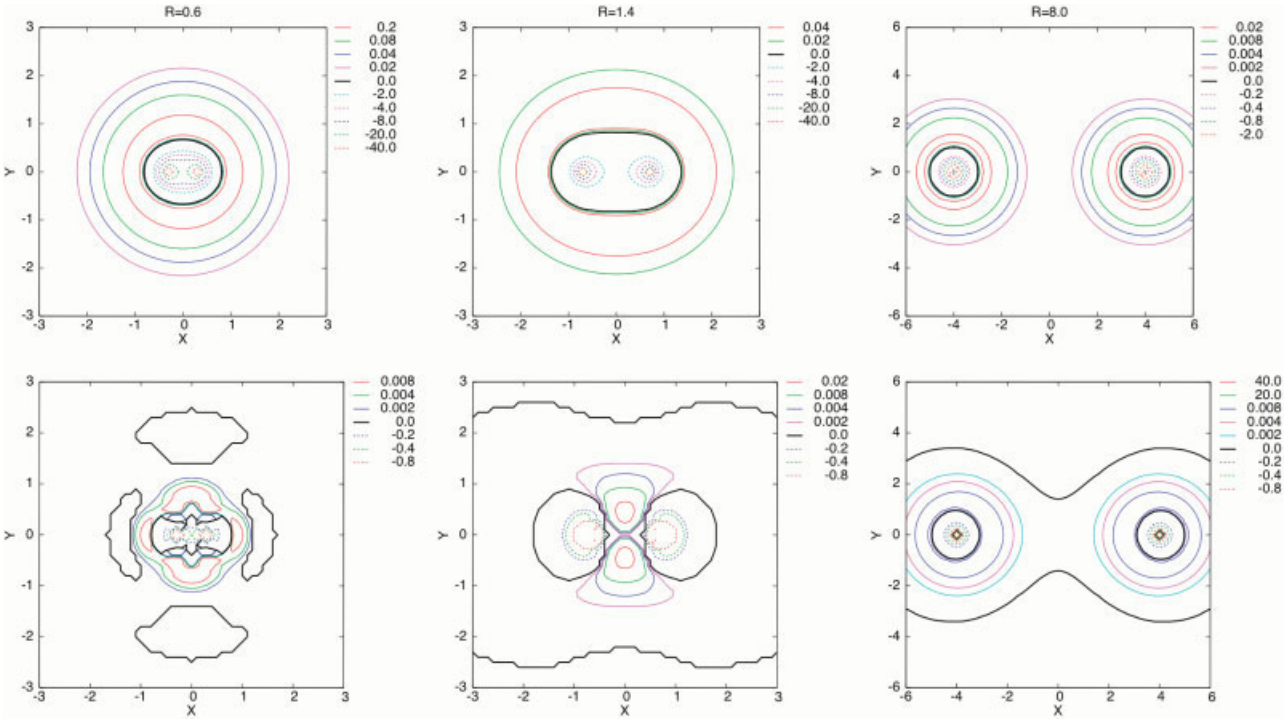

FIGURE 7. Plots of the H_2 ($X\ ^1\Sigma_g^+$) Laplacian of the electron density $\nabla^2_{\mathbf{R}}\,\rho(x, y, 0)$. The values in the top row are computed using Eq. (18), our largest Monte Carlo wavefunction and 64,000 Monte Carlo integration points. The values in the bottom row are the difference between our Monte Carlo results and the Laplacian of the electron density computed using a Hartree–Fock wavefunction. The atoms in this molecule are placed on the x-axis at $\pm R/2$. All values are in a.u. [Color figure can be viewed in the online issue, which is available at www.interscience.wiley.com.]

Along the internuclear axis the Laplacian of the extracule density has the same basic shape at each of the internuclear distances we investigated. The plots in Figure 9 have a negative local minimum at the origin, increases to a positive maximum and then drops to zero at large values of x. The main difference between our plot and the one in Ref. [17] is that the latter has lobes perpendicular to the internuclear axis i.e. the function reaches a positive maximum in this area. We see no evidence of this in our calculations.

If we again use the work of Fradera et al. [17, 26] to help interpret Figure 9, then the minimum at the origin represents a valence bond structure with one electron on each atom. Because this molecule is homonuclear and has only a single pair of electrons, the Laplacian of the extracule provides the same information as the extracule. For more complicated systems, like those in Ref. [26], this function can be used to help identify the different types of electron–electron interactions and map their most probable locations.

4. Calculating Hartree–Fock Densities

We can examine the influence of electron correlation on our expectation values by subtracting the result obtained with a Hartree–Fock wavefunction from the result obtained with our highly accurate Monte Carlo wavefunction. At each internuclear distance we generated a Hartree–Fock wavefunction by optimizing the exponents and positions of a large number of s-type Gaussians. The resulting energies (-0.72999 at $A_x = 0.3$, -1.13363 at $A_x = 0.7$ and -0.78650 at $A_x = 4.0$) are close to the Hartree–Fock limit. After a simple modification to our integral routines, we then calculated each expectation value. In Table II we list our results at nine points in the plane of the molecule, i.e. $\mathbf{R} = (x, y, 0)$. At $A_x = 0.3$ our Hartree–Fock values differ by an average of 15% with those obtained with our Monte Carlo wavefunction. As expected, I(0,0,0) has a large percentage difference (67%) because of the inability of

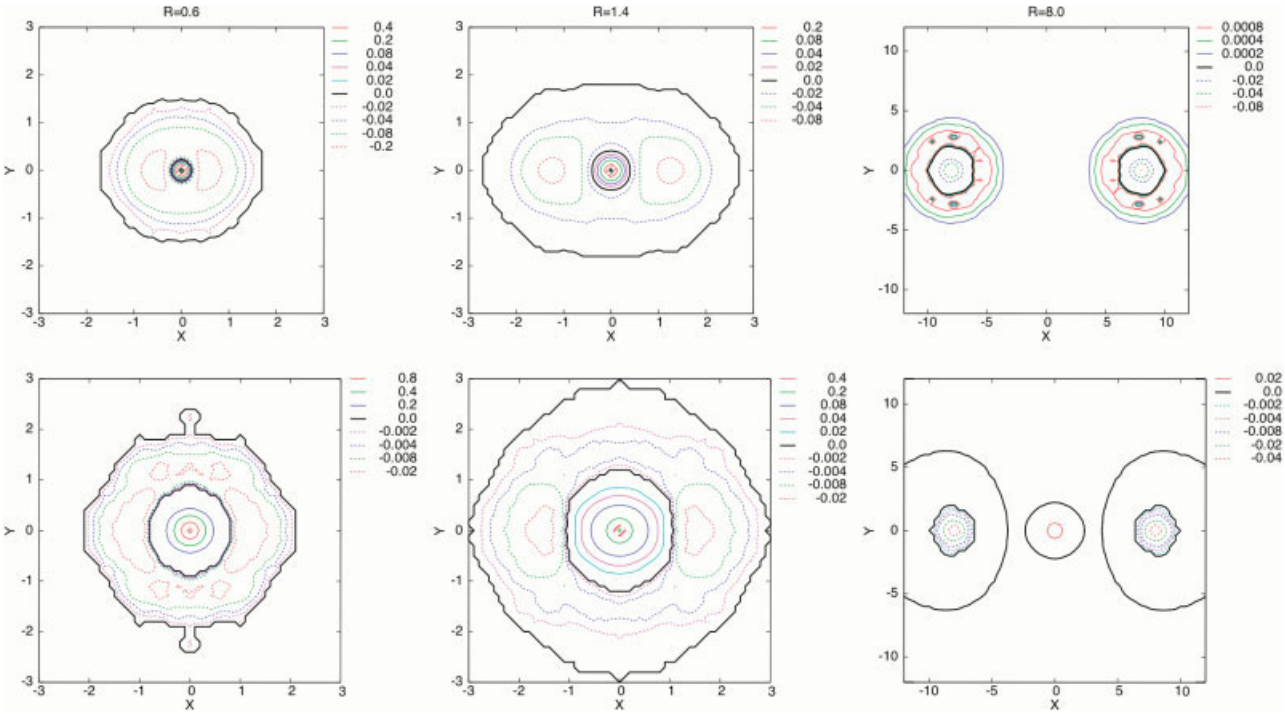

FIGURE 8. Plots of the H_2 ($X\ ^1\Sigma_g^+$) Laplacian of the intracule density $\nabla^2_{\mathbf{R}}\, I(x, y, 0)$. The values in the top row are computed using Eq. (19), our largest Monte Carlo wavefunction and 64,000 Monte Carlo integration points. The values in the bottom row are the difference between our Monte Carlo results and the Laplacian of the intracule density computed using a Hartree–Fock wavefunction. The atoms in this molecule are placed on the x-axis at $\pm R/2$. All values are in a.u. [Color figure can be viewed in the online issue, which is available at www.interscience.wiley.com.]

the Hartree–Fock wavefunction to correctly model the electron–electron cusp condition. The other intracule values have much smaller differences although their size slowly increases as **R** gets farther from the origin. Similarly, the extracule has a small difference near the origin and a steadily increasing difference as **R** gets larger. The largest difference occurs for the Laplacian of the intracule (50%) over a wide range of positions. The smallest differences occur for the electron density, the electron density difference and the Laplacian of the electron density. All of these properties have an average difference of 1% or less. At $A_x = 0.7$ the average difference increases slightly to 22%. The same general trends as before are the same here. At $A_x = 4.0$ there are substantial differences between many of our expectation values because the Hartree–Fock wavefunction ceases to be a good description of a molecule at large internuclear distances. Here, the average difference is 125%.

In Figures 1–9 we plot the differences between our Monte Carlo results and the Hartree–Fock results (the one exception is in Fig. 2 where we give only the difference between the Hartree–Fock electron density and the exact density). At small internuclear distances the differences tend to be minor. Not surprisingly, the greatest differences occur for the two particle functions, the intracule and extracule, showing clearly that electron correlation plays an important role. These differences are magnified for the Laplacians of these functions. At large internuclear distances all our functions show large differences because of the problems with the Hartree–Fock wavefunction.

5. Conclusions

Like the parable about the blind men describing an elephant, different quantum mechanical expectation values can be used to describe the distribution of electrons in a molecule. In this article we used explicitly correlated wavefunctions and variational Monte Carlo to calculate the values of the electron density, the electron density difference, the

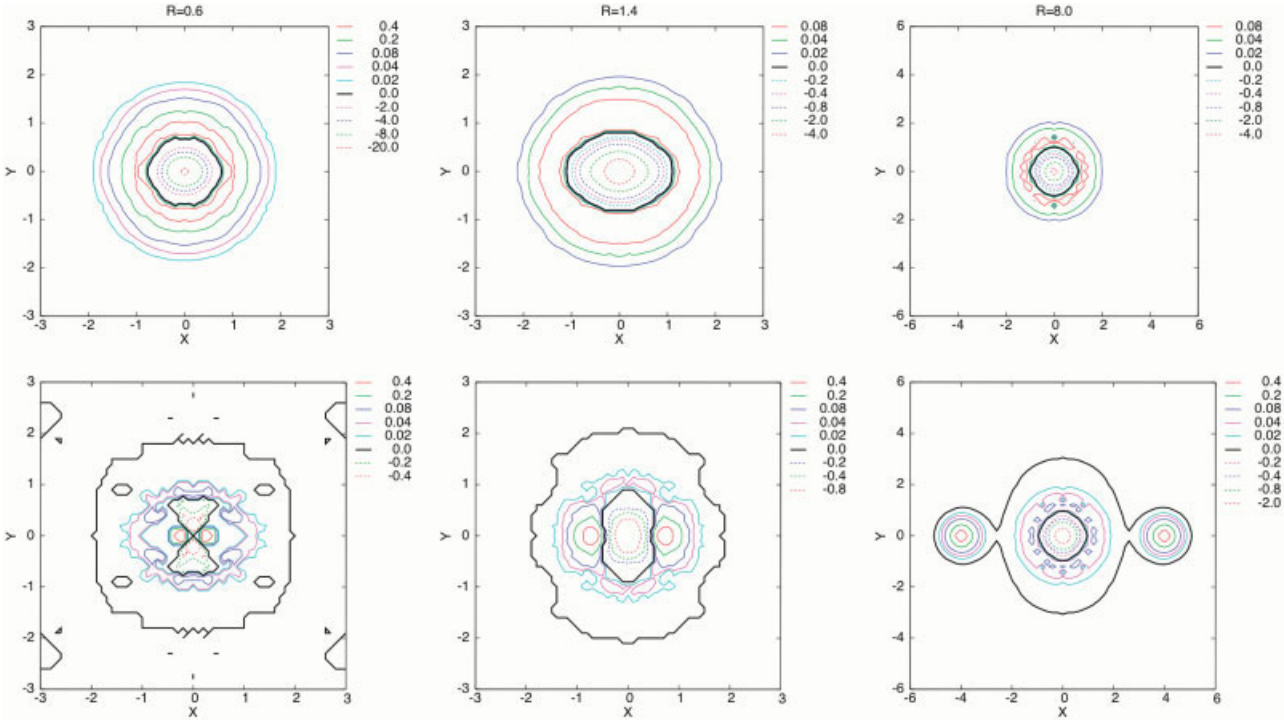

FIGURE 9. Plots of the H_2 ($X\ ^1\Sigma_g^+$) Laplacian of the extracule density $\nabla^2_{\mathbf{R}}\, E(x, y, 0)$. The values in the top row are computed using Eq. (20), our largest Monte Carlo wavefunction and 64,000 Monte Carlo integration points. The values in the bottom row are the difference between our Monte Carlo results and the Laplacian of the extracule density computed using a Hartree–Fock wavefunction. The atoms in this molecule are placed on the x-axis at $\pm R/2$. All values are in a.u. [Color figure can be viewed in the online issue, which is available at www.interscience.wiley.com.]

intracule density, the extracule density, two forms of the kinetic energy density, the Laplacian of the electron density, the Laplacian of the intracule density, and the Laplacian of the extracule density on a dense grid of points for the ground state of the hydrogen molecule at three internuclear distances. Our results clearly confirm the traditional molecular orbital view of this system—that it is a combination of both covalent and ionic structures at small internuclear distances and an ionic structure at large internuclear distances. We have also calculated these same properties using a Hartree–Fock wavefunction to examine the influence of electron correlation. In many cases, we find substantial differences between these calculations. In addition, we have shown that useful plots can be calculated with only a moderate number of Monte Carlo integration points. This suggests that this method can be successfully applied to larger molecules—systems whose expectation values will inevitably have higher statistical errors. Calculations on a variety of larger systems are now in progress.

ACKNOWLEDGMENTS

This project began because of the interest of Dr. Vedene Smith in molecular visualization techniques and we mourn his passing. The authors wish to thank Dr. Ajit Thakkar for several invaluable discussions and the staff of the Northeast Regional Data Center for their support in running our program on the University of Florida IBM NERSP.

References

1. Thakkar, A. J. In Density Matricies and Density Functionals; Erdahl, R., Smith, V. H., Jr., Eds.; Reidel: Dordrecht, 1987.
2. Bader, R. F. W. Atoms in Molecules: A Quantum Theory; Clarendon Press: Oxford, 1990.
3. Gillespie, R. J.; Popelier, P. L. A. Chemical Bonding and Molecular Geometry: From Lewis to Electron Densities; Oxford University Press: New York, 2001.
4. Becke, A. D.; Edgecombe, K. E. J Chem Phys 1990, 92, 5397.
5. Kulkarni, S. A. Phys Rev A 1994, 50, 2202.
6. Gill, P. M. W.; O'Neill, D. P.; Besley, N. A. Theor Chem Acc 2003, 109, 241.

7. Gill, P. M. W.; Crittenden, D. L.; O'Neill, D. P.; Besley, N. A. Phys Chem Chem Phys 2006, 8, 15.
8. Wang, J.; Tripathi, A. N.; Smith, V. H., Jr. J Phys B 1993, 26, 205.
9. Coldwell, R. L. Int J Quantum Chem 1977, S11, 215.
10. Alexander, S. A.; Coldwell, R. L.; Monkhorst, H. J.; Morgan, J. D., III. J Chem Phys 1991, 95, 6622.
11. Alexander, S. A.; Coldwell, R. L.; Morgan, J. D., III. J Chem Phys 1992, 97, 8407.
12. Alexander, S. A.; Coldwell, R. L. Int J Quantum Chem 2004, 100, 851.
13. Alexander, S. A.; Coldwell, R. L. J Chem Phys 2004, 121, 11557.
14. Alexander, S. A.; Coldwell, R. L. Int J Quantum Chem 2007, 107, 345.
15. Alexander, S. A.; Coldwell, R. L. Theochem 1999, 487, 67.
16. Moszynski, R.; Szalewicz, K. J Phys B 1987, 20, 4347.
17. Fradera, X.; Duran, M.; Mestres, J. J Phys Chem A 2000, 104, 8445.
18. Wolniewicz, L. J Chem Phys 1993, 99, 1851.
19. Pachucki, K.; Cencek, W.; Komasa, J. J Chem Phys 2005, 122, 184101.
20. Streitweiser, A., Jr.; Owens, P. H. Orbital and Electron Density Diagrams: An Application of Computer Graphics; Macmillan: New York, 1973.
21. Hongo, K.; Kawazoe, Y; Yasuhara, H. Int J Quantum Chem 2007, 107, 1459.
22. Das, G.; Wahl, A. C. J Chem Phys 1966, 44, 87.
23. Thakkar, A. J.; Tripathi, A. N.; Smith, V. H., Jr. Int J Quantum Chem 1984, 26, 157.
24. Alexander, S. A.; Coldwell, R. L.; Aissing, G; Thakkar, A. J. Int J Quantum Chem 1992, S26, 213.
25. Sarasola, C.; Dominguez, L.; Aguado, M.; Ugalde, J. M. J Chem Phys 1992, 96, 6778.
26. Fradera, X.; Duran, M.; Mestres, J. J Chem Phys 1997, 107, 3576.